Available online at www.sciencedirect.com
SCIENCE DIRECT®
Journal of Solid State Chemistry 177 (2004) 2079–2093
JOURNAL OF SOLID STATE CHEMISTRY
http://elsevier.com/locate/jssc

Investigation of cation environment and framework changes in silicotitanate exchange materials using solid-state ^{23}Na, ^{29}Si, and ^{133}Cs MAS NMR ☆

Brian R. Cherry,[a,*] May Nyman,[b] and Todd M. Alam[a]

[a] Department of Organic Materials, Sandia National Laboratories, P.O. Box 5800 MS0888, Albuquerque, NM 87185 USA
[b] Department of Geochemistry and the Department of Environmental Monitoring and Characterization, Sandia National Laboratories, Albuquerque, NM 87185 USA

Received 9 October 2003; received in revised form 6 February 2004; accepted 15 February 2004

Abstract

Crystalline silicotitanate (CST), $HNa_3Ti_4Si_2O_{14} \cdot 4H_2O$ and the Nb-substituted CST (Nb-CST), $HNa_2Ti_3NbSi_2O_{14} \cdot 4H_2O$, are highly selective Cs^+ sorbents, which makes them attractive materials for the selective removal of radioactive species from nuclear waste solutions. The structural basis for the improved Cs^+ selectivity in the niobium analogs was investigated through a series of solid-state magic angle spinning (MAS) NMR experiments. Changes in the local environment of the Na^+ and Cs^+ cations in both CST and Nb-CST materials as a function of weight percent cesium exchange were investigated using ^{23}Na and ^{133}Cs MAS NMR. Framework changes induced by Cs^+ loading and hydration state were investigated with ^{29}Si MAS NMR. Multiple Cs^+ environments were observed in the CST and Nb-CST material. The relative population of these different Cs^+ environments varies with the extent of Cs^+ loading. Marked changes in the framework Si environment were noted with the initial incorporation of Cs^+, however with increased Cs^+ loading the impact to the Si environment becomes less pronounced. The Cs^+ environment and Si framework structure were influenced by the Nb-substitution and were greatly affected by the amount of water present in the materials. The increased Cs^+ selectivity of the Nb-CST materials arises from both the chemistry and geometry of the tunnels and pores.

Keywords: Silicotitanate; Ion exchange; Selectivity; Cesium; Solid-state NMR

1. Introduction

The removal of radioactive ^{137}Cs or ^{90}Sr from nuclear defense waste is a high priority for the Department of Energy clean-up efforts. The radionuclides ^{137}Cs and ^{90}Sr are responsible for the majority of the radioactivity found in these waste solutions. Challenges to Cs^+ and Sr^{2+} removal include very high levels of dissolved salts and extremely basic (Hanford, SRS) or acidic (INEEL) waste solutions. Additionally, technologies for the removal of Cs^+ must be able to withstand high radioactive doses without diminishing performance. An inorganic ion exchanger material called crystalline silicotitanate (CST), $HNa_3Ti_4Si_2O_{14} \cdot 4H_2O$, developed in the early 1990s by Anthony and Dosch at Sandia National Laboratories [1–3], selectively sorbs 50 ppm Cs^+ from solutions containing ~5 M sodium salts. This CST material retains its stability and exceptional selectivity in both highly acidic and basic conditions as well as in radioactive environments. Furthermore, substitution of 25% of the framework Ti^{4+} with Nb^{5+} increases the selectivity for Cs^+ by approximately 14 times, as measured by the distribution coefficient [K_d, mL/g] [4] for Cs^+ over Na^+ [3,5]. Universal Oil Products (UOP LLC), in a cooperative agreement with Sandia, developed the Nb-substituted CST (Nb-CST), $HNa_2Ti_3NbSi_2O_{14} \cdot 4H_2O$, as a product known as IE910, and a granular form known as UOP IONSIV IE911™. Until August 2000, the addition of Nb^{5+} to the CST framework was a trade secret, protected by a US patent assigned to Sandia National Laboratories [1].

Recently, investigations into the structural mechanism responsible for the increased Cs^+ selectivity due to

☆ Supplementary data associated with this article can be found, in the online version, at doi: 10.1016/j.jssc.2004.02.020

*Corresponding author. Fax: +1-505-844-9624.
E-mail address: brcherr@sandia.gov (B.R. Cherry).

0022-4596/$ - see front matter © 2004 Elsevier Inc. All rights reserved.
doi:10.1016/j.jssc.2004.02.020

the addition of framework Nb^{5+} to the CST materials have been pursued. X-ray and neutron diffraction have been used by Clearfield et al. to study the structure of these materials [6–11]. The framework of CST is made up of $(TiO)_4$ cubane-like clusters that are linked by $SiO_{4/2}$ units, see Fig. 1. This arrangement results in a 3D structure with 8 Å diameter tunnels along the *c*-axis. Prior to exchange with Cs^+ ions, CST contains non-exchangeable and exchangeable Na^+ sites. The non-exchangeable Na^+ site is located in the *ac* crystal plane rigidly held by four silicate oxygen atoms and two water molecules. The exchangeable Na^+ (bonded to six waters) is located in the tunnels. Exchange with the tunnel Na^+ is kinetically favorable compared to the framework Na^+. In order to remove the framework Na^+, four strong Na–O–Si bonds must be broken. Conversely, the tunnel Na^+ is surrounded by labile H_2O. The ideal tunnel Cs^+ ion location forms eight bonds to silicate oxygen atoms. This bonding arrangement places the Cs^+ ion in the exact center of the tunnel and results in very normal Cs–O bond lengths [7,8]. Once a Cs^+ has exchanged into the tunnel site, the surrounding framework Na^+ are blocked from further exchange. From powder X-ray diffraction data, the framework structures of the CST material and the Nb-CST analog are indistinguishable, apart from a slight increase in unit cell size [6,11], and do not provide a definitive explanation for the improved Cs^+ selectivity. From these diffraction studies, Clearfield and co-workers conclude that there is more water in the tunnel of Nb-CST, increasing the water coordination to the Cs^+, which is a key factor in the improved Cs^+ selectivity.

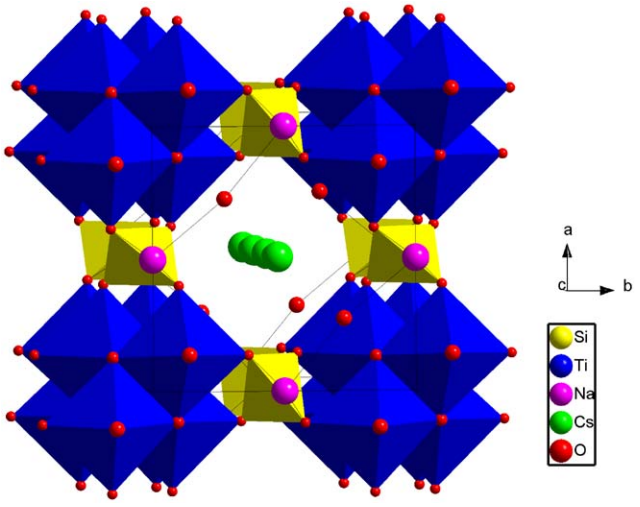

Fig. 1. Graphical representation of the crystal structure of CST ($HNa_3Ti_4Si_2O_{14}\cdot 4H_2O$), adapted from Poojary et al. [7]. The silicon atoms are depicted as light gray tetrahedra, the titanium as light gray octahedra, and the sodium as light gray spheres, cesium as dark gray spheres, and oxygen as black spheres. Extra cesium atoms are shown in the tunnel to illustrate potential binding sites. The non-framework sodium and water sites, present in the tunnel, are excluded for clarity.

Solid-state NMR has also been used to investigate these materials. Solid-state ^{93}Nb MAS NMR was recently performed by Cherry et al. [12], providing the first direct NMR study of the Nb environment in CST materials. For the Nb-CST material it was determined that the Nb is present in symmetric octahedra similar to the framework Ti octahedra it replaces [12]. Additionally, Luca et al. [13] studied the affects of replacing varying amounts of Ti with Nb in the CST material in the following system: $(HNa)_{2-y}Cs_yTi_{2-x}Nb_xSiO_7\cdot 2H_2O$ ($x = 0-2$; $y = 0.1-0.42$). X-ray diffraction, ^{29}Si and ^{133}Cs MAS NMR were used to characterize these materials. These studies also clearly demonstrated that for the CST and niobium analog materials the level of hydration played a role in the cation environments. Solid-state NMR is ideally suited to study these hydration effects, because the technique is very sensitive to changes in the local environments of the nuclei probed and does not rely on an average total structure, as with X-ray diffraction. The present investigation focuses on the Nb-CST analog that shows maximum Cs^+ selectivity, a composition Luca et al. [13] did not study.

The goal of this paper is to systematically investigate the structural basis for the improved Cs^+ selectivity of Nb-CST versus CST through careful solid-state NMR characterization of the framework structure and cation environments of these materials. Two series of materials were studied, the original CST material and the Nb-CST material, both with increasing Cs^+ loadings. The influence of hydration level on the framework structure and the cation environment were also investigated by comparing vacuum-dried samples to samples equilibrated under laboratory conditions.

2. Experimental section

2.1. Material preparation

Synthesis of Nb-substituted crystalline silicotitanate (Nb-CST), $HNa_2Ti_3NbSi_2O_{14}\cdot 4H_2O$: Titanium isopropoxide (TIPT, 3.43 g, 12 mmol), tetraethylorthosilicate (TEOS, 3.33 g, 16 mmol) and Nb_2O_5 (0.54 g, 4 mmol Nb) were added to 50 mL aqueous NaOH (6.6 g, 165 mmol) solution in a 100 mL Teflon liner to an autoclave Parr reactor. The mixture was stirred for 0.5 h, and then placed in a 200°C oven for 3 days. The resulting product, a white microcrystalline powder was collected by filtration (yield ~2.2 g of $HNa_2Ti_3NbSi_2O_{14}\cdot 4H_2O$; 86% yield based on Ti). A small amount of crystalline byproduct was inevitably formed with the major Nb-CST product. Before analyses of the sample, the byproduct was removed by a two step treatment: (1) the Nb-CST with the byproduct was first exposed to a 1 M aqueous HCl wash for three hours at room temperature, and (2) the Nb-CST with byproduct was

exposed to a 1 M NaOH wash for three hours at 40°C. The first step amorphizes the byproduct, and the second step dissolves the resulting amorphous byproduct.

Synthesis of crystalline silicotitanate (*CST*), $HNa_3Ti_4Si_2O_{14} \cdot 4H_2O$: The synthesis of CST materials was adapted from a previously published method [8]. Sodium hydroxide (6.6 g, 165 mmol) was dissolved in 50 mL of de-ionized water in a Teflon liner for a 100 mL stainless-steel autoclave. While stirring the NaOH solution, 4.56 g of titanium isopropoxide (Aldrich, 16 mmol) and 3.33 g of tetraethylorthosilicate (Aldrich, 16 mmol) were added. The precursor mixture was then seeded with 0.03 g of CST. The reaction mixture was then heated for 5 days at 200°C. The white microcrystalline powder (8.7 g) was filtered and washed with hot water to remove any NaOH residual. The yield was ~89% based on Ti (Si is in excess).

Cs^+ exchange: A series of Cs-exchanged Nb-CST and CST materials were prepared by ion exchange. The maximum amount of Na in Nb-CST that can be readily exchanged for Cs is approximately 25%. For each ion exchange, 3 g of Nb-CST was combined with 50 mL aqueous CsCl solution. The solution contained the appropriate amount of CsCl to produce Cs-exchanged Nb-CST samples with 3.8, 6.4, 9.0 and 9.6 wt% cesium incorporation. The Nb-CST/CsCl solutions were shaken at room temperature for 12 h, and the Cs-exchanged samples were collected by filtration. The series of Cs-exchanged CST materials, with 2.1, 3.3, 4.8, and 5.2 wt% Cs^+ incorporation, were prepared using the same method as the Nb-CST materials. Inductively Couple Plasma Mass Spectroscopy (ICP MS) was used for compositional analysis of these Cs-exchanged Nb-CST materials. ICP-MS analyses were carried out on PerkinElmer Sciex Elan 6100 instrument using an argon plasma flame and dual detector mode. Standards for linear regression curves for Na, and Cs (0.1–10 ppm) were made by appropriate dilution of 1000 ppm standards. Samples of CST (~50 mg) were dissolved in a few drops HF and diluted with DI H_2O to obtain Cs and Na concentrations within the range of the standards. Powder X-ray diffraction was used to examine phase identification, purity and crystallinity. The diffraction data were collected with a Bruker D8 Advance diffractometer in Bragg–Brentano geometry with Ni-filtered Cu$K\alpha$ radiation. Powder samples were loaded into a well-type sample holder. Data were collected from 5° to 60° with a step size of 0.05° and step time of 5 s.

2.2. Solid-state NMR analysis

The ^{23}Na and ^{133}Cs magic angle spinning (MAS) NMR experiments were performed on a Bruker Avance 600 at 158.75 and 78.72 MHz, respectively. In addition, ^{23}Na and ^{133}Cs MAS NMR spectra were collected on a Bruker AMX 400 at 105.85 and 52.49 MHz, respectively. For all investigations the MAS NMR spectra were collected using a 4-mm MAS broadband probe at a spinning speed of 12.5 kHz. For ^{133}Cs typical acquisition conditions included a 1.8 μs $\pi/6$ pulse (52.49 MHz) or a 1.0 μs $\pi/6$ (78.72 MHz) with respect to the $\pi/2$ pulse determined for 1 M CsCl, 1024 signal averages, and a 2 s recycle delay. For ^{23}Na typical acquisition conditions used were 1.5 μs $\pi/6$ pulse (105.85 MHz) or a 2.5 μs $\pi/6$ pulse (158.75 MHz), 64 scan averages with a 1 s recycle delay. For all ^{23}Na and ^{133}Cs MAS experiments high-power CW or two pulse phase modulation (TPPM) [14] ^1H decoupling were utilized. The ^{133}Cs and ^{23}Na NMR chemical shifts were referenced to the external secondary standards 1 M CsCl ($\delta = 0.0$ ppm) and 1 M NaCl ($\delta = 0.0$ ppm), respectively. The solid-state ^{29}Si NMR MAS and cross-polarization (CP)-MAS NMR experiments were collected on a Bruker AMX400 NMR spectrometer with a 7 mm broadband probe at a spinning frequency of 4 kHz. Typical direct single Bloch decay ^{29}Si NMR acquisition conditions included a 4.5 μs, $\pi/2$ pulse, TPPM ^1H decoupling [14], 128–432 scan averages, with a 240 s recycle delay. The typical CP-MAS ^{29}Si NMR acquisition conditions included a 5 ms contact pulse, TPPM ^1H decoupling, 1024 scan averages, with a 4 s recycle delay. Spectral deconvolutions were obtained using the extended version of Bruker WinFit and the Dmfit program written by Massiot [15–17]. The ^{23}Na MQMAS NMR spectra were collected at 105.85 MHz, utilizing the three pulse z-filtered MQMAS sequence [18], spinning at 12.5 kHz, with optimized pulse lengths of 5.2, 2.0, and 22.0 μs and a 2 s recycle delay.

Dried samples were prepared by drying under vacuum at 110°C for 7 days. The samples were then transferred to a glove box and packed in NMR rotors with tight fitting caps. All MAS NMR experiments were performed using dry N_2 as the spinning gas and the packed rotors were weighed before and after data collection to ensure that no weight gain due to water uptake had occurred. The as prepared samples were packed in rotors under ambient Albuquerque conditions without special precautions. During the time of year that the experiments were preformed the average relative humidity in Albuquerque, NM is 30–40% RH. As a point of comparison, during the same period the relative humidity in College Station, TX (the location of A. Clearfield's lab and site of most of the X-ray studies) is 60–80% R.H.

3. Results

3.1. As prepared samples

The solid-state ^{29}Si MAS NMR spectra for the as prepared CST and the Nb-CST materials as a function

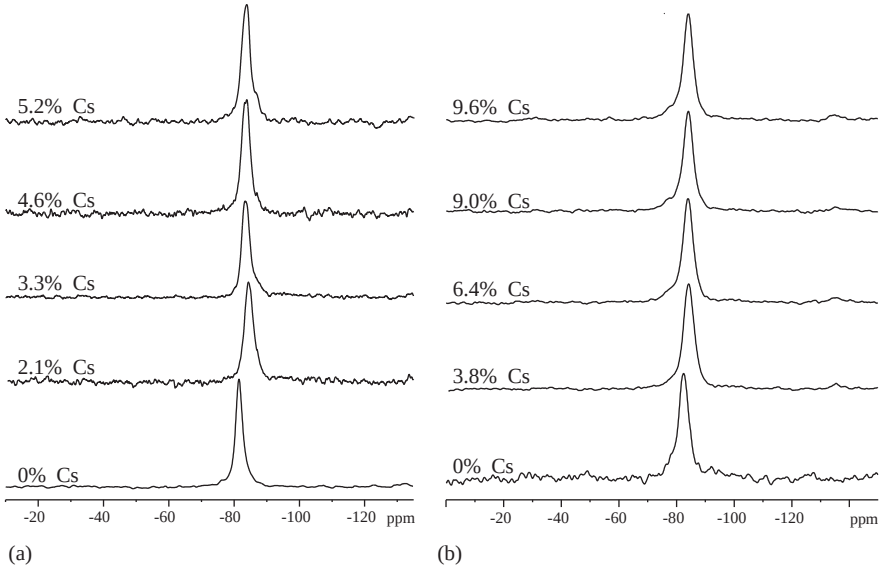

Fig. 2. The ^{29}Si MAS NMR spectra for the as prepared (hydrated). (a) CST and (b) Nb-CST materials as a function of wt% Cs^+ exchange.

of percent Cs^+ loading are shown in Fig. 2. The chemical shift, line width and relative fraction for each of the deconvoluted resonances are listed in Table 1. For the CST material, the ^{29}Si NMR spectrum for the end-group material (0% Cs) shows a single resonance at $\delta = -81.4$ ppm. For the Nb-CST with 0% Cs loading, a single resonance was observed at $\delta = -82.5$ ppm. With initial Cs^+ loading, the ^{29}Si NMR resonance shifts to $\delta = -84.3$ ppm for the CST (2.1 wt% Cs) material, and to $\delta = -83.7$ ppm for the Nb-CST (3.8 wt% Cs) material. Additional Cs^+ loading into either the CST material or the Nb-CST material has no additional effect on the ^{29}Si NMR chemical shift (see Table 1). For all samples the line width, full-width at half-maximum (FWHM) range between 200 and 300 Hz, with no FWHM trends observed as a function of Cs^+ loading. ^{1}H–^{29}Si CP MAS were also performed on all samples, CST shows an additional small impurity at $\delta = -83.7$ ppm (see supplemental material, Fig. S1).

The ^{23}Na MAS NMR spectra (at 105.85 MHz) for the as prepared (hydrated) CST and Nb-CST materials as a function of Cs^+ loading are shown in Figs. 3a and b, respectively. The ^{23}Na NMR chemical shift and line width for the CST and Nb-CST materials at two different magnetic field strengths are presented in Table 2. For the CST material containing no Cs^+ (0 wt%), only a single symmetric resonance was observed at $\delta = -3.6$ and -9.6 ppm at 158.75 and 105.85 MHz, respectively. For the Nb-CST material a single ^{23}Na resonance was observed at $\delta = -4.1$ and -10.0 ppm at 158.75 and 105.85 MHz, respectively. With increasing Cs^+ concentration, the ^{23}Na NMR resonance becomes asymmetric for the CST materials, while the Nb-CST materials remain a single symmetric resonance.

Table 1
Solid-state ^{29}Si MAS NMR parameters for as prepared (hydrated) CST and Nb-CST materials as a function of percent Cs^+ loading

	Cs (%)[a]	δ_{iso} (ppm ± 0.5)	FWHM (Hz)[b]
CST	0	−81.4	195
	2.1	−84.3	217
	3.3	−83.5	258
	4.6	−83.6	200
	5.2	−84.1	214
Nb-CST	0	−82.5	304
	3.8	−83.7	299
	6.4	−83.8	276
	9.0	−83.9	269
	9.6	−83.9	261

[a] Percent loading Cs refers to wt% Cs^+ content.
[b] FWHM : full-width at half-maximum.

By measuring the center of gravity (δ_{CG}) of the ^{23}Na NMR signal at two magnetic field strengths, an estimation of the quadrupole product (P_Q) can be determined using [16,19,20]:

$$\delta_{CG} = \delta_{iso} - \frac{P_Q^2}{40\upsilon_0^2} \quad \text{for } I = 3/2, \tag{1}$$

where δ_{iso} is the isotropic chemical shift and υ_0 is the observed Larmor frequency. Estimations of δ_{iso} and P_Q were determined from the δ_{CG} observed 1D ^{23}Na MAS NMR spectrum versus the inverse square of υ_0, and are given in Table 2.

The ^{23}Na multiple-quantum (MQ) MAS NMR spectra for the unexchanged CST material as well as the 5.2 wt% Cs loaded CST material are shown in Fig. 4. Fig. 5 shows the ^{23}Na MQMAS NMR spectra of the unexchanged Nb-CST and 3.8 wt% Cs Nb-CST

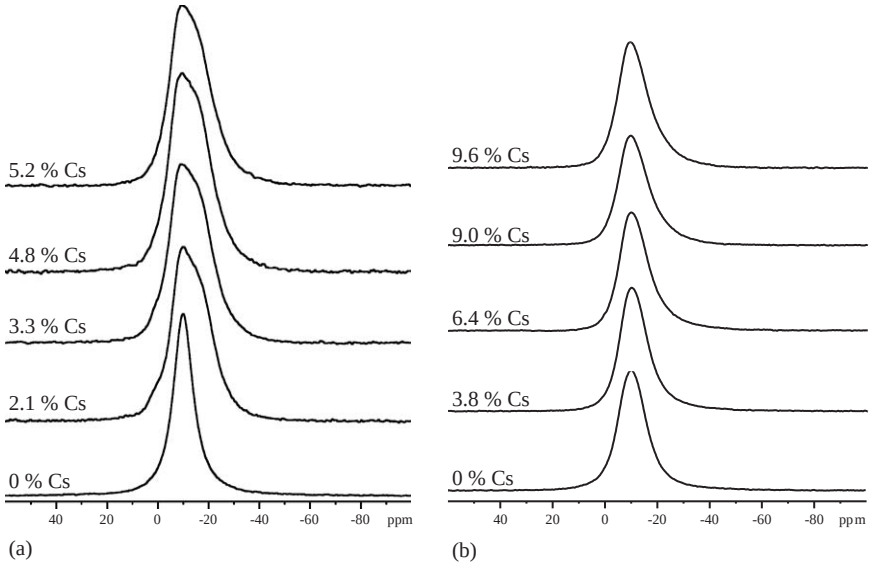

Fig. 3. The ^{23}Na MAS NMR spectra for the as prepared (hydrated). (a) CST and (b) Nb-CST materials as a function of wt% Cs^+ exchange. The NMR data was collected at the ^{23}Na observe frequency 105.85 MHz.

Table 2
^{23}Na MAS NMR fit parameters for the as prepared (hydrated) Cs^+ exchanged CST and Nb-CST materials

	Cs (%)[b]	105.85 MHz[a]		158.75 MHz[a]		δ_{iso} (ppm)[d]	P_Q (MHz)[d]	δ_{iso} (ppm)[e]	P_Q (MHz)[e]
		δ_{CG} (ppm)	FWHM (Hz)[c]	δ_{CG} (ppm)	FWHM (Hz)[c]				
CST	0	−9.6	1623	−3.6	1131	1.2	2.2	1.6	2.3
	2.1	−10.0	1742	−3.7	1214	1.3	2.3	—	—
	3.3	−9.2	1811	−3.7	1288	0.7	2.1	—	—
	4.8	−9.7	1820	−3.3	1284	1.8	2.3	—	—
	5.2	−9.3	1779	−3.1	1265	1.9	2.2	2.0	2.3
Nb-CST	0	−10.0	1332	−4.1	907	0.6	2.2	0.3	2.1
	3.8	−9.8	1296	−4.2	905	0.3	2.1	1.5	2.3
	6.4	−9.8	1358	−4.2	982	0.3	2.1	—	—
	9.0	−9.5	1415	−4.3	1051	−0.1	2.2	—	—
	9.6	−9.4	1445	−4.3	1080	−0.2	2.2	—	—

[a] ^{23}Na observation frequency.
[b] Percent loading Cs refers to wt% Cs^+ content.
[c] FWHM: full-width at half-maximum.
[d] As determined from field dependence of MAS δ_{CG} (center of gravity), see Eq. (1). Estimated error ±0.5 ppm.
[e] Determined from ^{23}Na MQMAS, estimated error in P_Q ±0.5 MHz.

materials. The spectra for all the samples studied, except the 5.2 wt% Cs CST material, shows a single resonance in the F_1 (isotropic) dimension. With Cs^+ exchange, an increase in the chemical shift dispersions is observed for the CST material. An additional resonance is observed in the isotropic dimension for the 5.2 wt% Cs CST sample, and is attributed to a small fraction of surface (hydrated) Na^+ (see Discussion).

The quadrupole interaction strength and isotropic chemical shift can be extracted from the sheared ^{23}Na MQMAS data using [21]:

$$\delta_{iso} = \frac{10}{17}\delta_2 + \frac{17}{27}\delta_1, \tag{2}$$

where δ_2 is the shift along the direct single quantum (F_2) dimension and δ_1 is the shift along the indirect multiple quantum (F_1) dimension after the shearing transformation. Values for P_Q were determined using [21]

$$P_Q = \left(\sqrt{\frac{680}{27}}\upsilon_0 \times 10^{-3}\right)\sqrt{(\delta_1 - \delta_2)} \tag{3}$$

and is related to quadrupolar coupling constant (C_Q) by

$$P_Q = C_Q\sqrt{1 + \frac{\eta_Q^2}{3}}. \tag{4}$$

The determination of the quadrupolar asymmetry parameter (η_Q) is ambiguous from the ^{23}Na MAS and

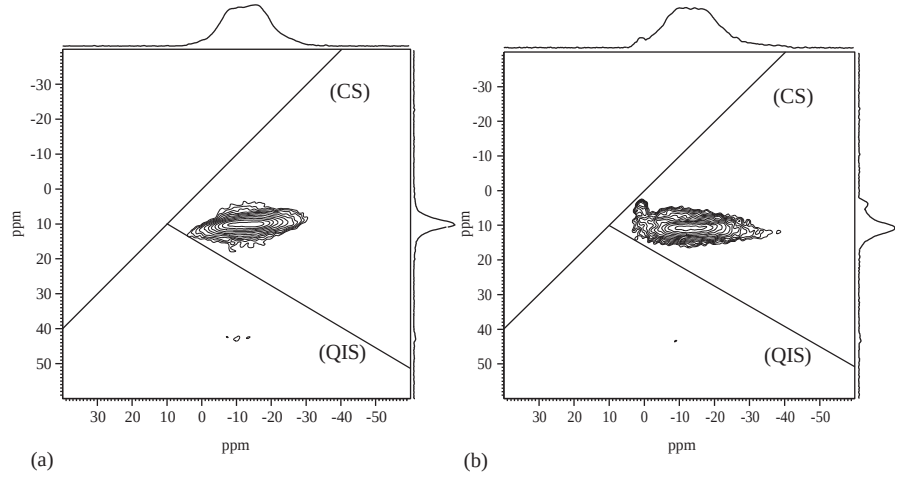

Fig. 4. The ^{23}Na MQMAS NMR spectrum, at 105.85 MHz, for the (a) CST material with 0 wt% Cs^+ and (b) 5.2 wt% Cs^+. The chemical shift (CS) and Quadrapolar Induced Shift QIS axis for the sheared MQMAS spectra are shown.

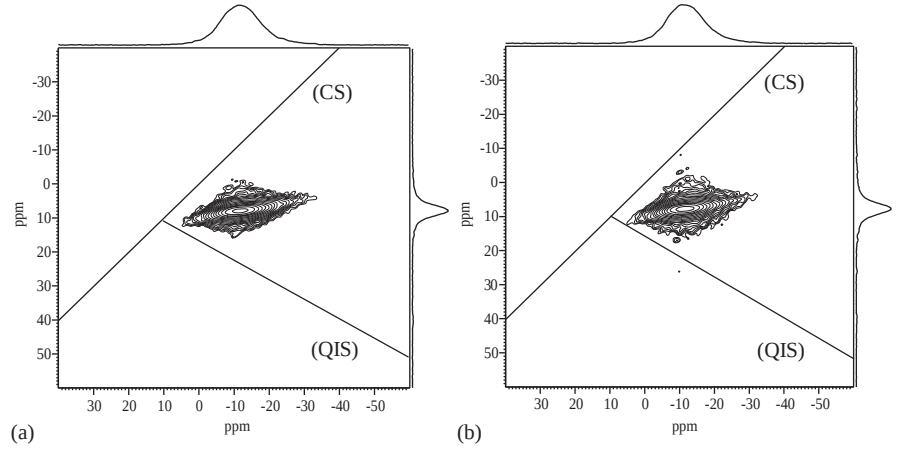

Fig. 5. The ^{23}Na MQMAS NMR spectrum, at 105.85 MHz, for the (a) Nb-CST material with 0% Cs^+ and (b) 3.8 wt% Cs^+.

MQMAS data. The largest effect η_Q will have on C_Q is ~16% error, therefore P_Q will be reported with the results listed in Table 2.

The ^{133}Cs MAS NMR spectra for the as prepared (hydrated) CST materials as a function of wt% Cs^+ loading are shown in Fig. 6a, while the ^{133}Cs MAS NMR spectra for the as prepared (hydrated) Nb-CST materials as a function of wt% Cs loading are shown in Fig. 6b. The ^{133}Cs spectra of the CST materials are made up of at least three resolvable Cs^+ environments (Table 3) with relative populations that are strongly dependent on the level of Cs^+ exchange. The ^{133}Cs chemical shift, line width, and relative fraction of the different resonances observed for the CST and Nb-CST materials are given in Table 3. The relative population of each ^{133}Cs resonance listed in Table 3 is based on integration of the complete spinning sideband manifold for each respective resonance. An example of the full ^{133}Cs NMR spectrum for the 3.3% Cs^+ CST material is shown in Supplemental Fig. S2.

3.2. Dehydrated samples

The ^{29}Si MAS NMR spectra of the dehydrated CST and Nb-CST samples are shown in Fig. 7 and the spectral parameters are listed in Table 4. The end member of the CST family (0% Cs) has a ^{29}Si NMR chemical shift $\delta = -78.0$ ppm. With initial Cs^+ loading, the ^{29}Si NMR resonance shifts to $\delta = -80.0$ ppm. An additional resonance, $\delta = -83.0$ ppm, was observed in the CST samples containing Cs^+. This resonance is accentuated by ^{1}H–^{29}Si CP-MAS NMR, indicating that the Si environment is strongly coupled to a proton that is not removed by the drying process (Fig. 8). In the Nb-CST samples, the end member (0% Cs) has a ^{29}Si NMR chemical shift $\delta = -78.9$ ppm. The ^{29}Si NMR of the materials containing Cs^+ are comprised of a main peak at approximately $\delta = -82.1$ ppm and a shoulder at $\delta = -79.5$ ppm. In both the CST and Nb-CST materials the ^{29}Si NMR spectra returns to that of the original hydrated materials

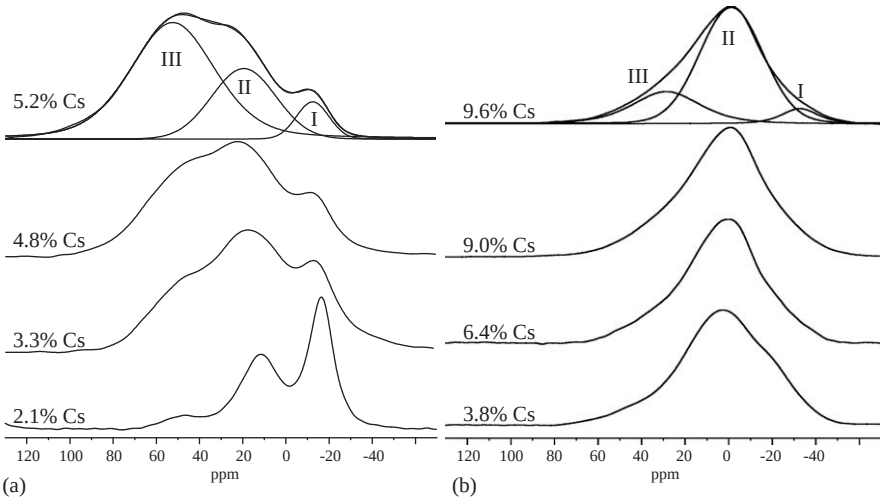

Fig. 6. The ^{133}Cs MAS NMR spectrum for the as prepared (hydrated) (a) CST and (b) Nb-CST materials as a function of wt% Cs^+ exchange. The top spectra shows an example of the spectral deconvolution, see Table 3.

Table 3
Solid-state ^{133}Cs MAS NMR parameters for the as prepared (hydrated) Cs^+ exchanged CST and Nb-CST materials

CST					Nb-CST				
Cs (%)[a]	Site	δ_{iso} (ppm)	FWHM (Hz)[b]	Area (%)	Cs (%)[a]	Site	δ_{iso} (ppm)	FWHM (Hz)[b]	Area (%)
2.1	I	−15.7	1045	52		I	−20	1540	26
	II	11.8	1935	45	3.8	II	4	1668	57
	III	49.0	1064	3		III	29	2360	17
3.3	I	−15.3	1337	36		I	−29	1120	7
	II	16.5	1831	45	6.4	II	0	1710	73
	III	49.3	1708	19		III	28	2020	20
4.6	I	−13.8	1110	22		I	−27	1620	13
	II	19.0	1933	49	9.0	II	−2	1530	44
	III	51.0	1983	29		III	15	2720	43
5.2	I	−12.3	943	11		I	−31	1270	7
	II	19.1	1788	40	9.6	II	−3	1590	48
	III	51.9	2450	49		III	15	2750	45

[a] Percent loading Cs refers to wt% Cs^+ content.
[b] FWHM: full-width at half-maximum.

when the samples are equilibrated to ambient atmospheric conditions (Fig. 2).

The ^{23}Na MAS NMR spectra of the dehydrated CST and Nb-CST samples are shown in Figs. 9a and b, and the spectral parameters are listed in Table 5. A decrease in the chemical shift and broadening of the resonance is observed for the vacuum dried materials.

The ^{133}Cs MAS NMR spectra of the dehydrated CST and Nb-CST samples are shown in Figs. 10a and b, and the spectral parameters are listed in Table 6. In both families of materials, the ^{133}Cs MAS NMR spectra are dominated by the Cs^+ species with the most negative chemical shifts. In CST, a broad resonance at approximately –10 to –15 ppm remains, while in the Nb-CST spectra two Cs^+ sites are observed. For Nb-CST the most positive chemical shift, $\delta = -14.9$ ppm, is dominant at low Cs^+ loading. As more Cs^+ is exchanged into the Nb-CST material the resonance with $\delta = -30.0$ ppm becomes the Cs^+ site with the highest relative population. The relative population of each ^{133}Cs NMR resonance listed in Table 6 is based on integration of the complete spinning sideband manifold for the respective resonances.

3.3. Variable temperature NMR

In an attempt to distinguish the different possible Na^+ sites predicted from crystallography, variable temperature ^{23}Na and ^{133}Cs NMR were also performed

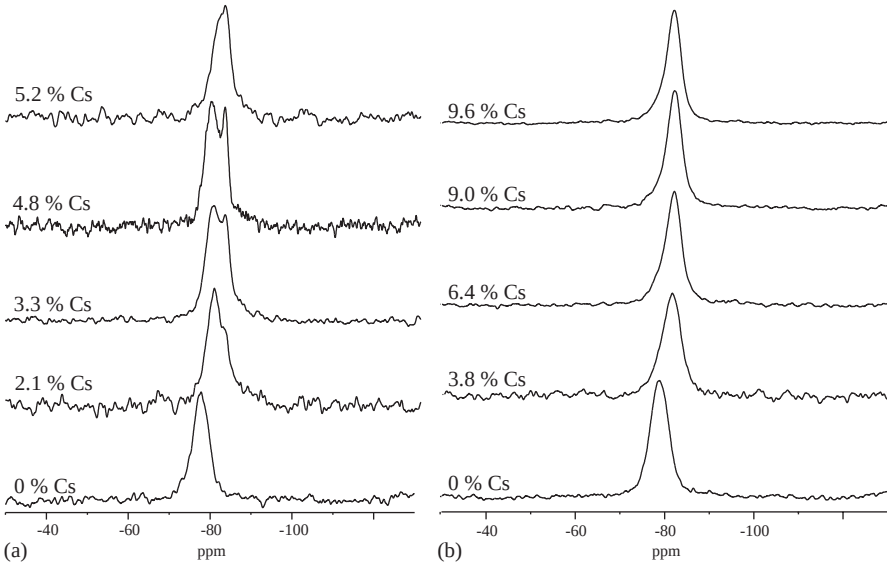

Fig. 7. The ^{29}Si MAS NMR spectrum for the dehydrated (a) CST and (b) Nb-CST materials as a function of wt% Cs^+ exchange.

Table 4
Solid-state ^{29}Si MAS NMR parameters for the dehydrated CST and Nb-CST materials as a function of percent Cs^+ loading

CST				Nb-CST			
Cs (%)[a]	δ_{iso} (ppm)	FWHM (Hz)[b]	Area (%)	Cs (%)[a]	δ_{iso} (ppm)	FWHM (Hz)[b]	Area (%)
0	−78.0	352	100	0	−78.9	359	100
2.1	−80.0	346	96	3.8	−81.3	379	100
	−83.0	88	4				
3.3	−79.9	298	54	6.4	−82.3	261	80
	−83.1	182	46		−79.3	326	20
4.6	−79.7	287	51	9.0	−82.4	265	84
	−82.9	169	49		−79.4	396	16
5.2	−81.2	299	53	9.6	−82.3	240	76
	−83.3	181	47		−79.7	398	24

[a] Percent loading Cs refers to wt% Cs^+ content.
[b] FWHM: full-width at half-maximum.

(see Figs. S3–S8 in the supplemental material). However, the distinction between the two known Na^+ environments was only observed at very high temperatures in the static ^{23}Na NMR spectrum. These different sodium sites were not observed in the high temperature ^{23}Na MAS NMR. The separation of the two sites is hampered by the very large line width ($\sim$50 ppm) observed from the high temperature ^{23}Na MAS NMR experiments. MAS spinning at high speeds and high temperature was not possible with our present probe capabilities. No high temperature ^{133}Cs NMR investigations were performed on the materials, since multiple Cs sites were resolved at room temperature.

4. Discussion

4.1. CST versus Nb-CST

4.1.1. Structural correlation based on solid-state ^{29}Si MAS NMR

The powder X-ray structures of the CST and Nb-CST materials are indistinguishable, apart from a slight increase in unit cell size [6–8]. NMR is sensitive to the electronic structure surrounding the nuclei probed and reveals minor differences in the two materials before Cs^+ loading takes place.

Extensive studies have been performed to correlate the experimental ^{29}Si NMR chemical shift with the

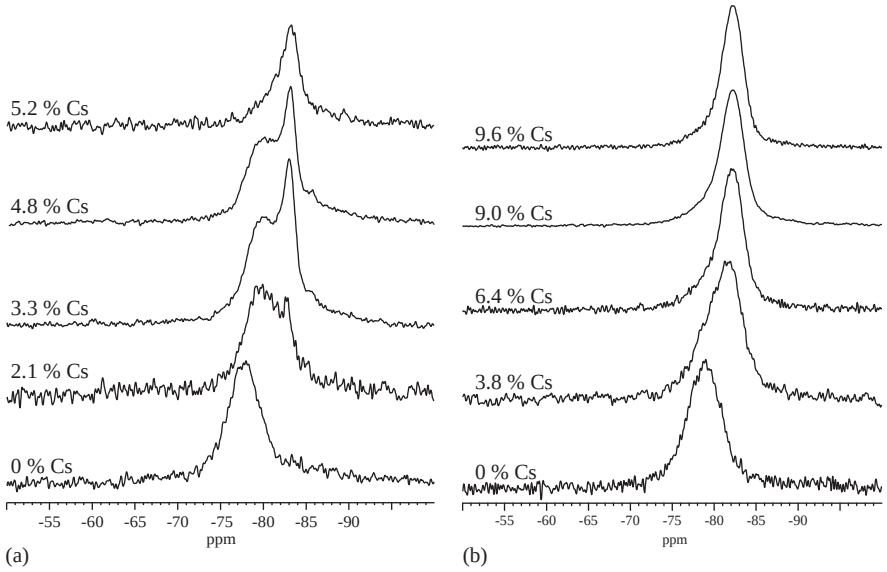

Fig. 8. ^{1}H–^{29}Si CP MAS spectra for the dehydrated (a) CST and (b) Nb-CST materials as a function of Cs^{+} loading. The lower frequency resonance more closely associated with protons is accentuated by cross polarization.

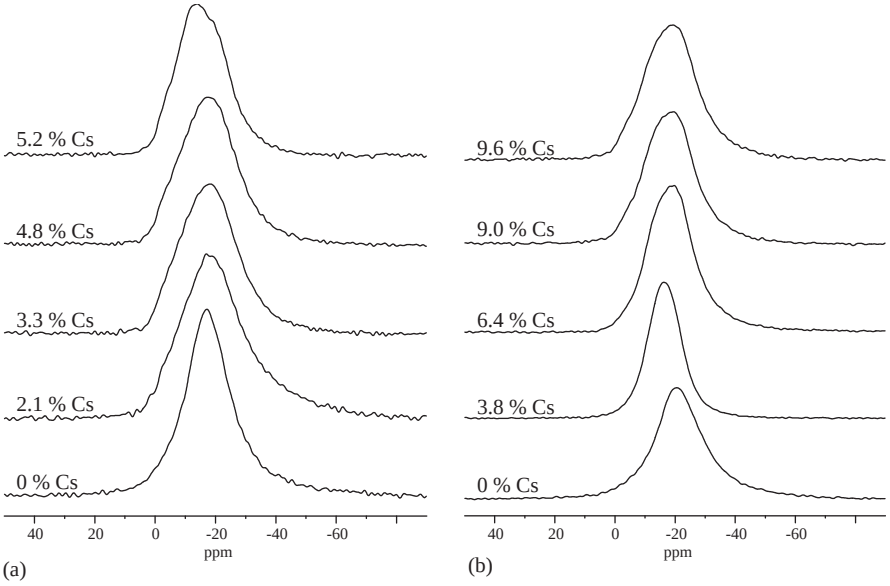

Fig. 9. The ^{23}Na MAS NMR spectrum for the dehydrated (a) CST and (b) Nb-CST materials as a function of wt% Cs^{+} exchange. The data was collected at 105.85 MHz.

structure of a material [22–24]. These approaches are derived from the ^{29}Si NMR chemical shifts of compounds with known crystal structures. The ^{29}Si NMR chemical shift is sensitive to Si–O bond lengths and angles, and to the chemical identity of the neighboring coordination sphere. A major limitation of these correlations is applying them to systems with extra framework cations [23]. The exact spatial relationship of the cations relative to Si atoms, are generally ill defined. The present system is no exception, in that the tunnel cations of the CST and Nb-CST materials are disordered. The picture is further complicated by the varying water content present in the materials. In spite

Table 5
^{23}Na MAS NMR fit parameters for the dehydrated Cs^{+} exchanged CST and Nb-CST materials at 105.85 MHz

CST			Nb-CST		
Cs (%)[a]	δ_{CG} (ppm)	FWHM (Hz)[b]	Cs (%)[a]	δ_{CG} (ppm)	FWHM (Hz)[b]
0	−17.2	1847	0	−20.4	1984
2.1	−17.0	2495	3.8	−16.5	1322
3.3	−17.5	2220	6.4	−18.5	1769
4.6	−17.5	2189	9.0	−18.3	1936
5.2	−13.7	1916	9.6	−19.4	2055

[a] Percent loading Cs refers to wt% Cs^{+} content.
[b] FWHM: full-width at half-maximum.

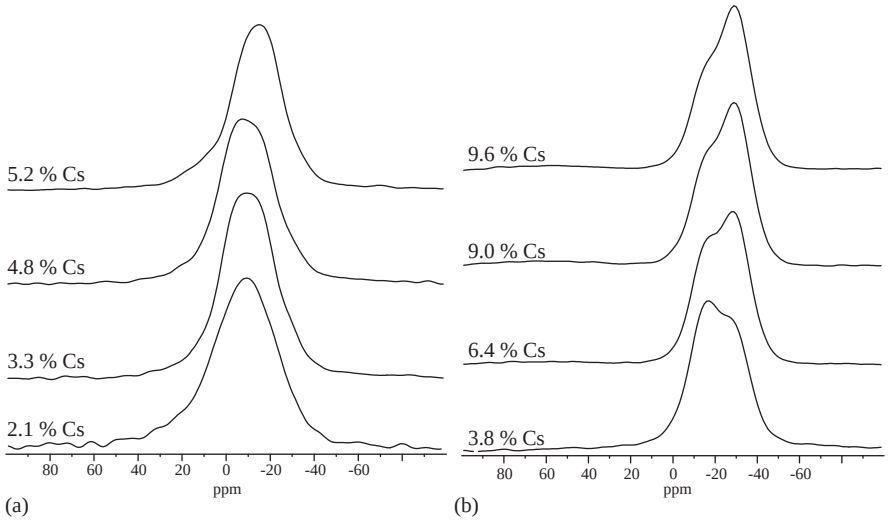

Fig. 10. The ^{133}Cs MAS NMR spectrum for the dehydrated (a) CST and (b) Nb-CST materials as a function of wt% Cs^+ exchange.

Table 6
^{133}Cs MAS NMR fit parameters for the dehydrated Cs^+ exchanged CST and Nb-CST materials

CST				Nb-CST				
Cs (%)[a]	Site	δ_{iso} (ppm)	FWHM (Hz)[b]	Cs (%)[a]	Site	δ_{iso} (ppm)	FWHM (Hz)[b]	Area (%)
2.1	I	−9.2	1770	3.8	I	−30.0	859	39
					II	−14.9	991	61
3.3	I	−10.0	1480	6.4	I	−30.0	890	55
					II	−14.9	860	45
4.6	I	−9.4	1510	9.0	I	−30.0	903	60
					II	−14.9	874	40
5.2	I	−14.1	1360	9.6	I	−30.0	933	64
					II	−14.9	859	36

[a] Percent loading Cs refers to wt% Cs^+ content.
[b] FWHM: full-width at half-maximum.

of these limitations, the ^{29}Si MAS NMR chemical shift provides valuable insights into how the Si environment changes with Nb incorporation, Cs^+ uptake, and hydration state.

In the materials studied here, there is a single dominant Si environment. In CST, the $SiO_{4/2}$ tetrahedra are directly linked to four $TiO_{6/2}$ octahedra and in close spatial proximity to the framework Na^+ and the Na^+/H_2O present in the tunnels (see Fig. 1). In the Nb-CST material 25% of the Ti atoms have been randomly replaced by Nb (disordered in the unit cell). The ^{29}Si NMR chemical shifts for the as prepared (hydrated) CST and Nb-CST materials are different, −81.4 and −82.5 ppm, respectively. The difference in electronegativity between Ti and Nb is not expected to play a role in the observed ^{29}Si chemical shift of the two classes of materials. If the electronegativity difference between Nb and Ti played a significant role influencing the ^{29}Si NMR chemical shift, multiple peaks or a pronounced broadening of the ^{29}Si resonance would be predicted in the Nb-CST material due to the presence of 25% of Si–O–Nb linkages and 75% Si–O–Ti linkages. Only a small difference in the CST and Nb-CST line width was observed (Table 1).

Since the electronegativity variation between Ti and Nb does not appear to influence the variation of the ^{29}Si NMR chemical shift, changes in either the mean Si–O bond length or the mean Si–O–Ti(Nb) bond angle may explain the change of chemical shift with Nb incorporation. Although not directly applicable to the silicotitanates of the present study, the relationships correlating ^{29}Si NMR chemical shift with structure of the Si sites can be used to infer the general structural change with Nb incorporation [22–24]. Confirming the validity of this assumption, Johnson et al. [24] have shown that the relationships that correlate Si–O bond length and Si–O–X bond angle with ^{29}Si chemical shift remain valid upon isomorphorus substitution of framework constituents. A more negative ^{29}Si chemical shift correlates with an increase in Si–O bond length and/or an increase of the

Si–O–X bond angle. Both of these changes would result in an increase in the size of the tunnel with Nb incorporation.

4.1.2. Variation in the Na^+ environment in CST and Nb-CST

For both the CST and Nb-CST materials, the ^{23}Na MAS NMR spectrum is a single, symmetric resonance. The similarity in ^{23}Na chemical shift suggests that there is not a large change in the Na^+ coordination environment between the two materials. However, the CST resonance is broader and has a slightly larger chemical shift as compared to the Nb-CST material, see Fig. 3 and Table 2. A portion of this broadening may reflect a dispersion in sodium environment, with the narrowing of the ^{23}Na resonance in the Nb-CST reflecting the reduction of the Na^+ concentration [6]. The loss of half of the tunnel Na^+ is required to charge balance the replacement of Ti^{4+} by Nb^{5+} in the framework of the Nb-CST materials. Exhaustive NMR experiments to resolve the framework and tunnel Na^+ were pursued, (see Supplemental Figs. S3–S8) but proved unsuccessful, except for very high temperatures. From a ^{23}Na NMR perspective, the similarity of the coordination environments of these two different Na^+ sites makes them hard to differentiate using NMR at the present magnetic field strengths and ambient temperatures. Both Na^+ sites are coordinated by six oxygen atoms. The only differences are the number of oxygen that are part of $SiO_{4/2}$ polyhedra and the number of oxygen from H_2O that coordinate the Na^+ [7,8].

4.2. The effect of Cs^+ loading in CST and Nb-CST

4.2.1. Variation in the ^{29}Si framework environment

The influence of Cs^+ loading environments on the framework were probed using solid-state ^{29}Si NMR. In the as prepared (hydrated) samples, Cs^+ loading has a varying effect on the framework of the CST and Nb-CST materials. In both materials the initial Cs^+ loading results in a decrease of the ^{29}Si NMR chemical shift (see Fig. 2, Table 1), but is invariant with further Cs^+ loading. Within experimental error (± 0.5 ppm), the ^{29}Si NMR chemical shifts of all the Cs^+ containing CST and Nb-CST materials are the same. This decrease in the chemical shift with initial Cs^+ loading is consistent with an increase of the Si–O bond length and/or an increase in the Si–O–Ti(Nb) bond angle. The decrease of the chemical shift is smaller for the Nb-CST material. The smaller changes in the Si–O–Ti(Nb) angle and the Si–O bond length suggest that there is a smaller perturbation in the size of the tunnels within the Nb-CST materials, perhaps suggesting the tunnels of the Nb-substituted materials more readily accommodate Cs^+ with minimal distortion, and thus the improve selectivity.

For any direct correlation to be made between the NMR predicted Si environment and that measured by crystallography, the level of hydration needs to be addressed. The level of hydration was defined in our work and the crystallography work of Tripathi et al. [6] as the ambient laboratory conditions. However, an appreciable variation in relative humidity is expected for the location of these respective studies. In Albuquerque at the time of the NMR experiments, the historical average relative humidity is 30–40% R.H. During the same period in College Station, TX (location of A. Clearfield's laboratory and site of most of the X-ray studies) the historical average relative humidity is 60–80% RH. The water present (or absent) in the tunnel has a more pronounced impact on the observed ^{29}Si NMR chemical shift (as discussed below).

4.2.2. Variation in cation environment

In the CST material, the ^{23}Na NMR resonance becomes asymmetric on the more negative ppm side (Fig. 3a) with increased Cs^+ exchange. No broadening of the symmetric ^{23}Na NMR signal is observed in the Nb-CST materials (Fig. 3b). P_Q measured for the CST materials is slightly larger than that measured for the Nb-CST materials and consistent with P_Q measured, more accurately, by ^{23}Na MQMAS NMR.

The ^{23}Na MQMAS spectra (Figs. 4 and 5) reveals that the asymmetric resonance in the 1D ^{23}Na MAS spectra of Cs-exchanged CST are due to an increase in the distribution of chemical shifts and C_Q. These distributions are deduced from the observed peak shapes of the MQMAS spectra. After the shearing transformation of the MQMAS spectra, a distribution in the chemical shift results in a spreading of the resonance along a line with a slope of one (CS), while a distribution in the quadrupolar induced shift (QIS) produces broadening of the resonance along a line with slope of $-10/17$ [21]. The CS and QIS axis are shown in Figs. 4 and 5 for clarity. For the CST material, the peak shape is characterized by a uniform quadrupolar C_Q and a small distribution in chemical shift (increased width of MQMAS resonance along the CS axis). The peak shape of the 5.2 wt% Cs CST material revealed an increase in the chemical shift distribution as well as a distribution of C_Q (increased width of MQMAS resonance along both the CS and QIS axis). This increase in both distributions reveals that the Cs^+ incorporation into CST impacts the local environment and symmetry of the Na^+ cations. No appreciable change in chemical shift distribution was observed in the 1D ^{23}Na MAS or ^{23}Na MQMAS spectra for Nb-CST materials. Both non-exchanged and Cs^+ containing materials exhibit broadening along the CS axis in the ^{23}Na MQMAS spectra, resulting from a small distribution of in the ^{23}Na chemical shift. This result indicates that the introduction of Cs^+ has almost no

impact on the local environment of the Na^+ cations in the Nb-CST materials. Table 2 lists the P_Q and isotropic chemical shift extracted from the MQMAS data utilizing Eqs. (2)–(4). In agreement with the field dependence of 1D ^{23}Na MAS NMR data, P_Q and the isotropic chemical shift are slightly larger for the CST materials. The increased P_Q reflects a more distorted environment around the sodium cations in the CST versus Nb-CST materials. The tunnel and framework Na^+ sites remain unresolved in the MQMAS spectra for both families of materials at ambient conditions. Under close inspection, the MAS line-shape and the single quantum (F2) projection of the MQMAS spectrum are not the same. This is due to non-uniform excitation of the full distribution of quadrupolar couplings present in the materials. This is a known artifact occasionally observed in MQMAS spectra [25]. More efficient multiple quantum excitation sequences such as fast-radiofrequency amplitude modulation (FAM) could be used to reduce this artifact [26–28]. To further emphasize the impact of a distribution of chemical shift has on a second-order quadrupolar line-shape, a simulation of a ^{23}Na MAS NMR spectrum with a 2 MHz C_Q was preformed. A Gaussian distribution of chemical shift was systematically added to the ^{23}Na MAS NMR spectrum. This simulation reproduces the asymmetric line-shape observed in the MAS spectra of the CST materials (supplemental Fig. S9).

The additional resonance that is resolved in the ^{23}Na MQMAS NMR spectrum of the 5.2% Cs CST material, Fig. 4b, is most likely due to a small fraction of surface (hydrated) Na^+ [29]. This species produces a small shoulder in the 1D ^{23}Na MAS NMR spectra of the Cs loaded CST materials. This resonance is not present in the 0% Cs CST material, nor the Nb-CST materials. The symmetric resonance is enhanced in the MQMAS spectrum due to differential MQ excitation/reconversion of different magnitude C_Q during the MQ pulse sequence. A qualitative estimate of concentration ($<2\%$) is obtained from integration of the 1D ^{23}Na MAS NMR spectrum.

The ^{133}Cs MAS NMR spectra (Fig. 6) are comprised of multiple ^{133}Cs resonances. In the CST materials, three resonances are resolved, as the Cs^+ content increases the relative populations shift to favor the adsorption/binding sites with larger chemical shift. These ^{133}Cs NMR results clearly show that at least three distinct Cs^+ environments are present in the CST exchanged materials. For each of the three resonances, a spinning sideband manifold was observed. Full simulation of the entire sideband manifold was used to extract the relative site fractions listed in Table 3. Additionally the breadth of the sideband manifold can be used to estimate the first-order quadrupole coupling, which was found to be approximately 170 ± 13 kHz for all three resonances (supplemental Fig. S2).

In contrast to the ^{23}Na NMR data, the ^{133}Cs chemical shifts do not have field dependence, indicating the second-order quadrupole interaction is vanishingly small for the Cs^+ in these materials. The X-ray structure only identifies two Cs^+ sites for equivalent materials (see Fig. 1) [8]. The Cs^+ is located in the center of the tunnel, and may take on various locations along the *c*-axis. The coordinating water molecules are not shown for clarity. The Cs^+ coordination number (CN) for these sites, based on the diffraction data, are 8 and 6, respectively [8]. To our knowledge, no correlations between ^{133}Cs NMR chemical shift and CN have been reported. The ^{133}Cs NMR is very sensitive to local Cs^+ environments and is able to distinguish subtle differences in the Cs^+ local bonding (in this case three binding environments) not resolved in the diffraction study.

In the Nb-CST materials, the ^{133}Cs MAS NMR spectra are much broader than the CST materials, but are still comprised of multiple resonances, indicative of multiple Cs^+ environments (Fig. 6). As with the CST materials each resonance has an associated spinning sideband manifold that was used to determine the relative fractions and estimate the first-order quadrupole coupling. The relative populations change slightly with Cs^+ content (Table 3).

Luca et al. [13] have previously reported that the ^{133}Cs NMR spectra of CST and Nb-CST materials are highly sensitive to water content, reflecting the diverse range of distinct water bonding environments. The water that surrounds each Cs^+ ion could take on a large number of slightly different coordinating arrangements producing a corresponding broad distribution of chemical shifts. The tentative assignment of the ^{133}Cs resonances are to Cs^+ located in the tunnel sites with a varying degree of hydrating water [13]. This impact of water on the Cs^+ distribution is confirmed by the ^{133}Cs NMR of the dried materials, discussed below.

Tripathi et al. [6] recently published X-ray powder diffraction results for Nb-CST with 4.0, 8.2, and 11.2 wt% Cs (based on reported formula). From their refinements, they determined that both CST and Nb-CST materials have two Cs^+ sites, Cs(1) and Cs(2). The principal difference between the CST and Nb-CST Cs^+ binding sites is an increase in the coordination number of the Cs^+ from 8 to 12 for Cs(1) and 6 to 10 for Cs(2). This increase in CN is possible because a portion of the tunnel Na^+ has been replaced by H_2O to charge balance the Nb^{5+} incorporation. The additional Cs^+ coordination is comprised of interactions with water molecules. In general, an increase in the coordination number of a cation will produce a decrease in the observed NMR chemical shift of that cation, as shown by Stebbins and co-workers [30–34] for ^6Li, ^{23}Na, and ^{25}Mg in a variety of crystalline, glassy, and molten materials. The cation-oxygen bond length and oxygen valence also influence

the chemical shift, as described by Koller and co-workers [35]. The center of gravity of the ^{133}Cs MAS NMR spectra of the Nb-CST materials has a more negative chemical shift, relative to the CST materials. Assuming the Cs–O bond lengths do not change significantly, the ^{133}Cs NMR results are consistent with an increase in the Cs^+ CN with Nb incorporation.

4.3. The effect of drying

Thermal gravimetric analysis (TGA) data for the CST and Nb-CST materials are shown in the supplemental information (Fig. S10). The TGA data reveals two thermal events attributed to the loss of water. The drop in the TGA, prior to 180°C, indicates the loss of loosely or phys-adsorbed water (3–4 wt%), while the event between 200°C and 350°C accounts for the loss of the tightly bound tunnel H_2O (an additional 6–8 wt%). Comparison of the TGA data for CST and Nb-CST (0% Cs) reveals that the loose or physi-adsorbed water content is slightly more in Nb-CST, but the removal of the tightly bound tunnel water is similar in both materials. The slope of the TGA curve, during the loss of the tunnel H_2O, for the Nb-CST materials containing Cs^+ is less steep compared to the CST and 0 wt% Cs^+ Nb-CST materials. This suggests that the removal of the tunnel H_2O is hindered by the presence of Cs^+ in the Nb-CST materials.

As referred to in the previous sections, dehydration of the CST and Nb-CST materials has a pronounced effect on both the framework structure and cation environment. Following dehydration, the ^{29}Si NMR chemical shift is globally shifted to larger values due to the loss of H_2O. In the base CST material (0% Cs), the ^{29}Si chemical shift increases 3.4 ppm upon drying. The ^{29}Si NMR spectra of the CST materials containing Cs^+ are comprised of two resonances after drying, at approximately –80 and –83 ppm (Table 4). Upon re-hydration, the framework of CST materials return to their former structure, indicated by the ^{29}Si NMR spectrum returning to that of the original (hydrated) sample ($\delta = -84.3$). Powder X-ray diffraction of the re-hydrated samples also confirms that the structural change upon dehydration is reversible. We assign the more positive (−80 ppm) resonance to the fully dehydrated CST material. The other sharper resonance is very close to the ^{29}Si NMR chemical shift of the hydrated CST materials. Therefore, this resonance is assigned to the ^{29}Si environment in the CST material that was incompletely dehydrated. ^{1}H–^{29}Si CPMAS NMR accentuates this resonance, indicating that this Si environment is more strongly associated with protons (from H_2O or –OH), (see Fig. 8). The change in ^{29}Si NMR chemical shift indicates a structural change of the CST material upon dehydration. Dehydration induced structural changes have been observed in other almuminosilicate and titanosilicate materials. Engelhardt and co-workers [36] showed the effects of re-hydration on dehydrated hydrosodalite. Zibrowius et al. [37] have recently shown that the framework of the titanosilicate ETS-10 is altered by the presence of polar sorbates, e.g. H_2O, methanol, and ammonia. The observation of changes in the diffraction pattern with hydration supports the argument that the ^{29}Si chemical shift variation is structurally related and not due to susceptibility effects. The 3.4 ppm increase in the ^{29}Si NMR chemical shift of the dehydrated CST material suggests large decrease in the Si–O–Ti bond angle upon dehydration (compared to the increase of this angle with Nb or Cs^+ incorporation).

Solid-state ^{29}Si NMR analyses of the Nb-CST materials also suggested reversible structural changes upon dehydration and re-hydration. As with the CST materials, a global shift to larger ^{29}Si chemical shift values upon dehydration is observed. The increase of 3.6 ppm in the ^{29}Si NMR chemical shift indicates a slightly larger decrease in Si–O–Ti(Nb) bond angle (compared to the dehydration of CST). The ^{29}Si MAS NMR spectra of the Cs^+ containing Nb-CST materials are asymmetric on the downfield side of the resonance. The shoulder around $\delta = -79.5$ ppm is assigned to dehydrated Nb-CST material. However, a large fraction ($\sim$80%) of the ^{29}Si NMR signal remains at $\delta = -82.1$ ppm. This is assigned to slightly dehydrated material, indicating that it is much harder to remove the water present in the tunnels of Nb-CST when the material contains Cs^+. The TGA data supports this interpretation (Fig. S10).

With drying, there is decrease in chemical shift and broadening of the ^{23}Na MAS NMR spectra. The Nb-CST materials are affected more strongly than the CST materials, an additional 3 ppm shift to more negative values and an additional 200 Hz increase in line width, suggesting that the cation hydration has a larger impact for the Nb-CST materials.

The level of hydration of the CST and Nb-CST materials also plays an important role in the distribution of Cs^+ sites populated by the absorbed Cs^+ during exchange. In the CST materials that were equilibrated to laboratory conditions, at least three resolvable Cs^+ sites are observed (see Fig. 6a). As the Cs^+ exchange level increases, the relative population of the Cs^+ sites with larger chemical shifts increases. The ^{133}Cs NMR data for the dried materials (Fig. 10) reveals that the Cs^+ environments with more negative chemical shift becomes the dominant species. As discussed in Section 4.2.2, increasing the CN of a cation, results in a more negative chemical shift [30–34], assuming the Cs–O bond lengths do not change significantly. This indicates that the Cs^+ coordination number increases with dehydration of the CST and Nb-CST materials. Cs^+ has a high affinity for water, therefore it is logical to think that any water remaining in the material after the dehydration preformed would be tightly associated with the Cs^+.

The breadth of the sideband manifold increases as well indicating a slight increase in the first-order quadrupolar coupling (225 ± 14 kHz, supplemental Fig. S2). The increase of the quadrupole coupling is indicative of local distortions of the Cs^+ environment upon dehydration. The magnitude of the coupling increase suggests the distortions are not large. However, little is known about the influence of local distortion on the ^{133}Cs first-order quadrupole coupling.

In the dehydrated Nb-CST materials, two Cs^+ sites are observed (Fig. 10b) whose relative populations reverse as a function of Cs^+ loading (Table 6). These results show that dehydration has populated the Cs^+ species with the more negative chemical shift (see Tables 3 and 6) consistent with increasing the Cs^+ coordination. With increased Cs^+ loading the concentration of this higher coordinate Cs^+ environment increases. As in the CST materials, the first-order quadrupolar coupling slightly increases after drying (225 ± 14 kHz).

Tripathi et al. [6] concluded from their structures determined from X-ray data that the increased coordination by water is responsible for the observed increase in Cs^+ selectivity. The solid-state NMR data presented in this paper compliments and solidifies these conclusions. The broader ^{133}Cs NMR spectra of the hydrated Nb-CST materials, compared to the CST materials as indicated by the line width (Tables 3 and 6), indicates a higher degree of dispersion in the hydration (as discussed in Section 3.2). After drying, the Cs^+ site with the most negative shift observed (-30 ppm) is populated in the Nb-CST materials. This large negative ^{133}Cs chemical shift is not observed in the CST materials, suggesting that the Nb-CST materials have a higher Cs coordination number. Additionally, the behavior of the ^{29}Si NMR spectra with dehydration indicates that the removal of water is more difficult in the Nb-CST materials that contain Cs^+.

5. Summary and conclusions

A series of solid-state NMR studies were conducted to provide insights into variations of the CST and Nb-CST materials upon Cs^+ exchange. The incorporation of Nb^{5+} into CST has ramifications on not only the framework structure of the material but also on the nature of the cation binding sites. From the ^{29}Si NMR data, it was concluded that the framework structure of the base (0% Cs^+) Nb-CST material closely matches the structure of Cs^+ exchanged materials, while larger structural variations are observed in the CST materials with Cs^+ incorporation. The Nb-CST has a slightly larger unit cell [6] which can more easily accommodate the large Cs cation with less framework expansion. From this viewpoint, Cs^+ selectivity is greater in Nb-CST than CST because the energetics of accommodating a Cs^+ is more favorable for Nb-CST in that it involves a smaller framework expansion. Subtle differences in the ^{23}Na NMR data indicates that the depopulation of the tunnel Na^+ sites to charge compensate for the Nb^{5+} incorporation in the framework of the materials. The incorporation of Cs^+ perturbs the Na^+ environment less in the Nb-CST versus the CST material. With these observations, Cs^+ selectivity of Nb-CST over CST can be viewed as a matter of less repulsion from nearby cations in the tunnel, as well as ease of site hopping for the Cs^+, once it has entered the tunnel. These effects should increase the kinetics of Cs^+ exchange in the Nb-CST phase, as well as increase the stability of the Cs^+ at its tunnel site (less repulsion). The ^{133}Cs NMR data provides a direct measure of the multiple Cs^+ binding environments inside the tunnels of the materials. The ^{133}Cs NMR data reflects the increase level of local hydration present in the tunnels and corresponding increase in Cs^+ coordination number of the Nb-CST materials. This data suggests the increased selectivity of Cs^+ in the Nb-CST phase arises from stabilization of the exchanged-in Cs^+ by increased coordination within the tunnel site.

X-ray diffraction data of complex crystalline solids such as the CST materials gives an average snapshot of framework atoms and tunnel occupants. However, some details cannot be determined accurately such as occupation of mixed sites, chemistry and geometry of mobile tunnel species, and subtle framework changes that are influenced by changes in the tunnel sites. Additionally, very light atoms such as hydrogen often cannot be located at all. Multinuclear NMR techniques are very useful for filling in such structural detail, as well as for providing additional insight into geometry and binding specific to particular atoms. Since NMR is atom specific, low concentrations and mixed occupancies do not dilute or mask the information gained from this technique. For these reasons, we were able to provide a characterization complementary to X-ray characterization of CST, Nb-CST, and Cs^+ substituted and dehydrated variations of both. A number of arguments for the increased Cs^+ selectivity with Nb-substitution into the CST framework were revealed by these studies. This study and the predecessor studies of Tripathi et al. [6] and Lucca et al. [13] have yielded consistent evidence for the origin of high Cs^+ selectivity in these important ion exchange materials. The Cs^+ selectivity arises from both chemistry and geometry of the tunnels and pores, and these investigations have given insight to how new materials might be tailored for ion exchange specificity.

Acknowledgments

Sandia is a multiprogram laboratory operated by Sandia Corporation, a Lockheed Martin Company, for

the United States Department of Energy's National Nuclear Security Administration under contract DE-AC04-94AL85000.

References

[1] R.G. Anthony, R.G. Dosch, C.V. Phillip, Sandia National Laboratories, USA, 1995.
[2] R.G. Anthony, C.V. Philip, R.G. Dosch, Waste Manage. 13 (1993) 503–512.
[3] D. Gu, Kinetics Catalysis and Reaction Engineering Laboratory, Department of Chemical Engineering, Texas A&M University, College Station, TX, 1995.
[4] Z. Zheng, C.V. Philip, R.G. Anthony, J.L. Krumhansl, D.E. Trudell, J.E. Miller, Ind. Eng. Chem. Res. 35 (1996) 4246–4256.
[5] R.G. Dosch, R.G. Anthony, Sandia National Laboratories, Albuquerque, NM, 1995.
[6] A. Tripathi, D.G. Medvedev, M. Nyman, A. Clearfield, J. Solid State Chem. 2003, accepted for publication.
[7] D. Poojary, A. Bortun, L. Bortun, A. Clearfield, Inorg. Chem. 35 (1996) 6131–6139.
[8] D. Poojary, R. Cahill, A. Clearfield, Chem. Mater. 6 (1994) 2364–2368.
[9] P. Pertierra, M. Salvado, S. Garcia-Granda, A. Bortun, A. Clearfield, Inorg. Chem. 38 (1999) 2563–2566.
[10] A.I. Bortun, L.N. Bortun, D.M. Poojary, O. Xiang, A. Clearfield, Chem. Mater. 12 (2000) 294–305.
[11] A. Clearfield, Solid State Sci. 2 (2001) 103–112.
[12] B.R. Cherry, M. Nyman, T.M. Alam, in: S.K. Sundaram, D.R. Spearing, J.D. Vienna (Eds.), Environmental Issues & Waste Management Technology in the Ceramic & Nuclear Industries VIII, Ceramic Transactions, Vol. 143, The American Ceramics Society, Westerville, OH, 2003, pp. 377–384.
[13] V. Luca, J.V. Hanna, M.E. Smith, M. James, D.R.G. Mitchell, J.R. Bartlett, Microporous Mesoporous Mater. 55 (2002) 1–13.
[14] A.E. Bennett, C.M. Rienstra, M. Auger, K.V. Lakshmi, R.G. Griffin, J. Chem. Phys. 103 (1995) 6951–6958.
[15] M.E. Smith, Bruker Rep. 1 (1990) 33–35.
[16] M.E. Smith, F. Taulelle, D. Massiot, Bruker Rep. 2 (1990) 16–18.
[17] D. Massiot, F. Fayon, M. Capron, I. King, S. Le Calvé, B. Alonso, J.O. Durand, B. Bujoli, Z. Gan, G. Hoatson, Magn. Res. Chem. 40 (2002) 70–76.
[18] S.P. Brown, S.J. Heyes, S. Wimperis, J. Magn. Res. A 119 (1996) 280–284.
[19] K.T. Mueller, Y. Wu, B.F. Chemlka, J. Stebbins, A. Pines, J. Am. Chem. Soc. 113 (1991) 32.
[20] J.H. Baltisberger, S.L. Gann, E.W. Wooten, T.H. Chang, K.T. Mueller, A. Pines, J. Am. Chem. Soc. 114 (1992) 7489.
[21] J.P. Amoureux, C. Huguenard, F. Engelke, F. Taulelle, Chem. Phys. Lett. 356 (2002) 497–504.
[22] G. Engelhardt, D. Michel, High-Resolution Solid-State NMR of Silicates and Zeolites, Wiley, Chichester, 1987, pp. 77–157.
[23] A. Labouriau, T.J. Higley, W.L. Earl, J. Phys. Chem. B. 102 (1998) 2897–2904.
[24] G.M. Johnson, P.J. Mead, S.E. Dann, M.T. Weller, J. Phys. Chem. B. 104 (2000) 1454–1463.
[25] M. Zeyer, L. Montagne, V. Kostoj, G. Palavit, D. Prochnow, C. Jaeger, J. Non-Cryst. Solids 311 (2002) 223–232.
[26] A.P.M. Kentgens, R. Verhagen, Chem. Phys. Lett. 300 (1999) 435.
[27] P.K. Madhu, A. Goldbourt, L. Frydman, S. Vega, Chem. Phys. Lett. 307 (1999) 41.
[28] P.K. Madhu, A. Goldbourt, L. Frydman, S. Vega, J. Chem. Phys. 112 (2000) 2377.
[29] H. Du, V.V. Terskikh, C.I. Ratcliffe, J.A. Ripmeester, J. Am. Chem. Soc. 124 (2002) 4216–4217.
[30] X. Xue, J.F. Stebbins, Phys. Chem. Miner. 20 (1993) 297–307.
[31] Z. Xu, J.F. Stebbins, Solid State Nucl. Magn. Res. 5 (1995) 103–112.
[32] J.F. Stebbins, Solid State Ionics 112 (1998) 137–141.
[33] A.M. George, S. Sen, J.F. Stebbins, Solid State Nucl. Magn. Res. 10 (1997) 9–17.
[34] P.S. Fiske, J.F. Stebbins, Am. Miner. 79 (1994) 848–861.
[35] H. Koller, G. Engelhardt, A.P.M. Kentgens, J. Sauer, J. Phys. Chem. 98 (1994) 1544–1551.
[36] G. Engelhardt, J. Felsche, P. Sieger, J. Am. Chem. Soc. 114 (1992) 1173–1182.
[37] B. Zibrowius, C. Weidenthaler, W. Schmidt, Phys. Chem. Chem. Phys. 5 (2003) 773–777.